# Spatial and temporal variability of Atlantic Water in the Arctic from observations

**Alice E. Richards**[1], **Helen L. Johnson**[1], **Camille Lique**[2]

[1]Department of Earth Sciences, University of Oxford, Oxford, United Kingdom
[2]Université de Bretagne Occidentale, CNRS, IRD, Ifremer, Laboratoire d'Océanographie Physique et Spatiale, IUEM, Brest, France

**Key Points:**

- Atlantic Water (AW) evolution differs in the eastern and western Arctic and will likely lead to distinct future regimes in the two basins
- Interaction between the AW and cold dense shelf flows may be an important mechanism through which AW loses heat
- AW core temperature is effective in assessing AW heat content but core depth does not always reflect AW layer depth

Corresponding author: Alice Richards, `alice.richards@stx.ox.ac.uk`

## Abstract

Atlantic Water (AW) is the largest reservoir of heat in the Arctic Ocean, isolated from the surface and sea-ice by a strong halocline. In recent years AW shoaling and warming are thought to have had an increased influence on sea-ice in the Eurasian Basin. In this study we analyse 59000 profiles from across the Arctic from the 1970s to 2018 to obtain an observationally-based pan-Arctic picture of the AW layer, and to quantify temporal and spatial trends. The potential temperature maximum of the AW (the AW core) is found to be an easily detectable, and generally effective metric for assessments of AW properties, although its depth is not always a good indicator of the depth of the AW layer. In contrast to the Eurasian Basin, where the AW warms in a pulse-like fashion and has an increased influence on upper ocean heat content, AW heat in the Canadian Basin became more isolated from the surface due to the intensification of the Beaufort Gyre and an influx of Pacific Water. The increase in density of the AW core suggests an increasing interaction between cold dense shelf flows and the AW during its advection, consistent with the enhanced brine rejection expected from decreases in summer sea-ice extent. This process could play an important role in AW cooling west of the Lomonosov Ridge. The differences in AW trends in the Eurasian and Canadian Basins of the Arctic over the period studied suggest that these two regions may evolve differently over the coming decades.



## Plain Language Summary

A few hundred meters beneath the surface of the Arctic Ocean lies a warm, salty layer of Atlantic origin, referred to as Atlantic Water (AW), which is isolated from the surface by a strong vertical salinity gradient (halocline). In the eastern Arctic in recent years, halocline weakening and warming AW have contributed to unprecedented sea-ice loss. In this study, we analyse 59000 temperature and salinity profiles from the Arctic Ocean from the 1970s to 2018 to obtain a pan-Arctic picture of the AW and its variability. The temperature maximum of the AW is found to be an easily observable, generally effective way to assess AW heat. Over the period studied, the AW in the eastern Arctic warmed in a pulse-like fashion and had an increasing influence on the amount of heat in the surface layer, whereas AW heat became increasingly isolated from the surface in the west due to changes in local winds and water masses. The AW also became cooler and denser in the western Arctic due to enhanced interaction with cold salty flows from the shelves. The emergence of a characteristically different eastern and western Arctic Ocean in the future could have important consequences, both regionally and globally.


## 1 Introduction

Beneath the cool, fresh surface layer of the Arctic Ocean lies a warm, saline intermediate layer of Atlantic origin. This Atlantic Water (AW) flows in through the Fram Strait (as the Fram Strait Branch) and the Barents Sea (as the deeper, cooler Barents Sea Branch) and travels cyclonically around the Arctic as a topographically steered boundary current following the continental slope, with part of the current recirculating along the Lomonosov and Alpha-Mendeleev Ridges into the interior and back towards the Fram Strait (Aksenov et al., 2011; Woodgate et al., 2001). It eventually exits the Arctic into the North Atlantic via the Canadian Arctic Archipelago (CAA) and the Fram Strait, fresher and cooler than it came in, having taken about 20-30 years to complete its journey (Lique et al., 2010; M. J. Karcher & Oberhuber, 2002; Rudels, 2015; Wefing et al., 2020). Heat is transferred from this AW boundary current to the interior via intrusions and eddies (McLaughlin et al., 2009; Kuzmina et al., 2011).

The AW layer is the most significant reservoir of heat in the Arctic Ocean (Carmack et al., 2015), therefore changes in its temperature could have a significant impact on the Arctic region. The AW layer currently contains enough heat to melt all Arctic sea-ice within just a few years if this heat were brought to the surface in that time (Turner, 2010), although across most of the Arctic the AW is isolated from the sea-ice and surface mixed layer by a strong halocline. Observations suggest that AW temperature variations are dominated by low-frequency oscillations with a period of 50-80 years, linked to changes in the Nordic Seas which are advected through the Fram Strait (Polyakov et al., 2004). Superimposed on these low-frequency oscillations are inter-annual pulse-like temperature variations which enter through the Fram Strait or St Anna Trough and are advected with the boundary current (M. J. Karcher et al., 2003; Schauer et al., 2002; Dmitrenko et al., 2008; Polyakov et al., 2004; McLaughlin et al., 2009). There was also a net warming trend in AW temperature over the twentieth century (Polyakov et al., 2004, 2012), and AW in the Fram Strait is now unprecedentedly warm compared to the last two millennia, with a rapid temperature increase in the upper AW layer over the last 120 years (Spielhagen et al., 2011).

In the eastern Eurasian Basin, recent increases in AW temperature, along with associated shoaling of the AW and a weakening halocline, have enhanced vertical heat transfer from the AW to the surface layer and have resulted in a substantial reduction in winter sea-ice formation (Lind et al., 2018; Polyakov et al., 2010, 2017). This "Atlantification" of this region shows how important a role AW can play in a changing Arctic. Furthermore, Atlantification and resultant sea-ice reduction can affect the AW itself in a variety of ways. The reduction of sea-ice import to the Barents Sea can cause a local increase in AW temperature, salinity, and hence density (Barton et al., 2018) and can also result in local convection which has consequences for the AW layer downstream (Lique & Steele, 2012; Lique et al., 2018). In the Eurasian Basin, reduced ice cover and a resultant increase in ventilation is expected to cause local decreases in AW temperature and salinity (Pérez-Hernández et al., 2019). The impact of these local AW changes on the wider Arctic region is not yet fully understood, but is another important part of the changing role AW can play in the future Arctic environment.

Downstream in the Canada Basin the impact of AW on sea-ice is currently observable at the margins of the Canada Basin, with AW upwelling here (caused by wind) linked to local sea-ice reduction (Ladd et al., 2016). Changes in both sea-ice cover and the intensity of the Beaufort Gyre in the interior Canada Basin can affect the AW (Lique & Johnson, 2015; Lique et al., 2015). The recent spin-up of the gyre resulted in a deepening of the underlying AW due to Ekman pumping, and a shoaling of the AW temperature maximum at the gyre margins (Zhong & Zhao, 2014). The pathway and intensity of AW in the Canada Basin are affected by the surface circulation here as well (M. Karcher et al., 2012; Lique et al., 2015).

Changes to the AW also have consequences outside of the Arctic. It is thought that the low density of the present warm AW anomalies in the Arctic could be maintained throughout their circumnavigation of the Arctic Ocean, and hence reduce the density of outflows into the North Atlantic (M. Karcher et al., 2011). The properties of the boundary current and these deep outflows that are advected into the North Atlantic have the potential to significantly influence overturning in this region - an important component of the global climate system.

Understanding how AW heat is likely to change in the future is therefore a key part of predicting what will happen to the Arctic in the years to come. There is large discrepancy and bias amongst coupled climate model representations of AW in the Arctic, with the AW layer generally being too deep and thick. The AW temperature biases are primarily due to inaccurate representation of sea ice coverage and surface cooling in the Barents Sea, formation of cold and dense water in the Barents Sea, and AW inflow temperatures through the Fram Strait (Shu et al., 2019; Ilıcak et al., 2016). It is therefore particularly important to have an observational description of AW to help evaluate these models, given their use in predicting future Arctic changes.

Oceanic observations in the Arctic are sparse and often seasonally biased, and many observational studies of the Arctic focus on specific regions or transects (e.g. Anderson et al. (1994); Beszczynska-Moller et al. (2012); Li et al. (2020); Lind et al. (2018); McLaughlin et al. (2009); Polyakov, Rippeth, et al. (2020)). However, the number of Arctic Ocean observations has increased in recent years. This study aims to synthesise data from various sources across the Arctic from the 1970s to 2018 to give a pan-Arctic, up-to-date description of the AW layer and its impact on the water column. Diagnostics derived from these observations, such as the temperature, salinity and depth at the AW temperature maximum (the AW core) and AW heat content are used to characterise the spatial and temporal variability of the AW and are described in section 2. The spatial variability of the AW properties is investigated in section 3, with temporal variability in both the eastern and western Arctic described in section 4. Observed changes in AW and heat distribution within the water column at moorings and at repeated CTD transects are discussed in section 5. Finally, section 6 explores the relationship between AW core properties and other metrics used to assess the state of the AW layer.

## 2 Data and Methods

Conductivity-temperature-depth (CTD) observations from across the Arctic are used in this study, from four different sources: the ice-tethered profiler (ITP) program (Toole et al. (2011); Krishfield et al. (2008), `http://www.whoi.edu/itp`) and the Beaufort Gyre Exploration Project (BGEP, `https://www.whoi.edu/beaufortgyre`) - both based at the Woods Hole Oceanographic Institution - the Nansen and Amundsen Basins Observational System (NABOS, `https://uaf-iarc.org/nabos`), and data from the NOAA World Ocean Database (WOD, `https://www.nodc.noaa.gov/OC5/WOD/pr\_wod.html`). The WOD collates oceanic observational data from a wide range of sources. The WOD data used here are those from CTD profiles, drifting buoys, and ocean stations. Any ITP, BGEP or NABOS data were removed from the WOD dataset before use to avoid duplication. The BGEP and NABOS datasets include data from both moorings and ship surveys.

Throughout the paper, salinity is given in Practical Salinity Units, and potential temperature (when not available directly from the observational data product), heat content and potential density are computed using the Thermodynamic Equation of Seawater 2010 (TEOS-10) (IOC et al., 2010).

All data used in this study are processed versions of the raw data gathered in the field. Details of these procedures can be found in the sources referenced above, but all involved calibration, sensor-correction and the removal or flagging of obviously erroneous data. In addition to this initial processing, further routines were applied to the data and profiles were smoothed for much of our analysis - details of which are given below. Profiles with more than 10 % of data masked or flagged as suspicious were omitted from the analysis and, unless otherwise stated, monthly mean data from moorings were used so as not to bias any regional analysis to the mooring locations due to the relative high sampling frequency here compared to other locations. This resulted in about 59000 profiles for analysis.

As density is driven by salinity in the Arctic, the potential temperature of the AW can be seen as a passive tracer. The potential temperature maximum of the AW layer, herein referred to as the AW core, is commonly used to follow the circulation and transformations of AW (M. J. Karcher et al., 2003). The AW core in a given profile is defined as the maximum potential temperature in the portion of the profile with salinity greater than 34.7 (in order to avoid surface temperature maxima), following Lique and Steele (2012). Figure 1 shows the distribution in time and space of profiles where the AW core was identified, with mooring locations shown as black squares.

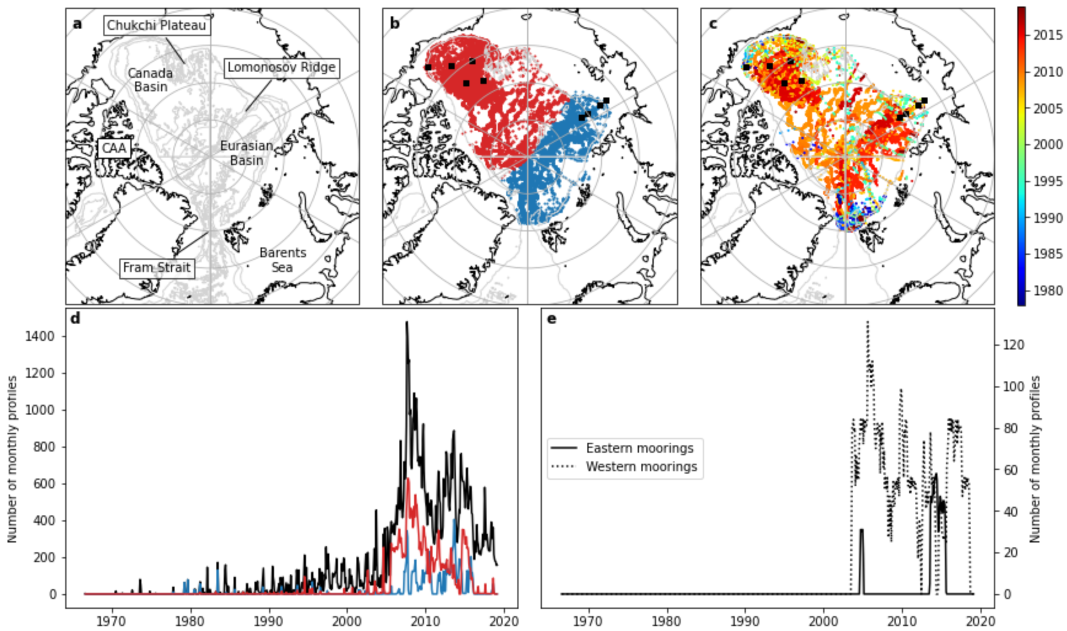


**Figure 1.** (a) Map of the Arctic with bathymetric contours for every 1000 m shown along with relevant geographic features. (b) Spatial distribution of all AW core data points coloured by region, with east in blue, west in red, and mooring locations marked with black squares. (c) Spatial distribution of all AW core data points coloured by the year in which the measurements were obtained. (d) Time series showing number of monthly profiles, with east in blue, west in red and all Arctic data in black (some of which lay outside of both the eastern and western regions, so are not shown on map or used in analysis). (e) Time series showing number of monthly mooring profiles in the eastern and western regions.

To ensure the AW core identified in each profile was not an artefact of limited sampling, profiles were required to start above 100 m and cover a depth range of at least 500 m before being used to identify the AW core (this also eliminated data from the surrounding shelf seas, allowing the study to focus on AW within the Arctic basin only). This latter step resulted in about 44000 AW core data points. Before identifying the core, profiles were smoothed over a vertical distance of 80 m by taking the mean of the profile data within 40 m of each data point. This length scale was chosen as it was the best at preserving the general shape and magnitude of the temperature profile, while removing the spikes due to features such as thermohaline intrusions and eddies (although please note that this smoothing was not applied to the profiles in Figure 3). This is important as the main aim of this study is to get a general picture of AW core patterns and long-term trends, and features such as intrusions can disproportionately affect the *depth* of the AW temperature maximum in basin interiors in such a way as to detract from this. Any profiles used in the analysis should be assumed to be smoothed unless stated otherwise.

The depth coverage varies between data sources - ITP profiles cover the upper 800 m of the water column, whereas many data from CTD stations and moorings extend down to around 2000 m. This variation in depth range does not affect the analysis in this study given that the AW core can be identified in both cases, and any profiles that do not sample the whole AW layer are omitted from the AW heat content analysis in section 6. Although ITPs and moorings provide year-round measurements, there remains a spring/summer bias to data from other sources. However, this is unlikely to impact results due to the negligible seasonality of AW when compared to its overall variability in space and time (Lique & Steele, 2012).

The AW layer itself was defined as the portion of the water column bounded by the 0°C potential temperature crossing points either side of the AW core.

Heat content, HC, was computed for various portions of the vertical temperature profiles according to

$$HC = \int_a^b \rho_\theta(z) c_p T(z)\, dz$$

where $\rho_\theta$ is potential density, $c_p$ is specific heat, $T$ is potential temperature, and $z$ is depth (with $a$ and $b$ being the depth bounds defining the layer in question). 1500 profiles sampled the entire AW layer and allowed for the computation of total AW heat content. To account for differing profile lengths above the AW layer (due to variation in upper depths of profiles and the depth of the AW layer itself), heat content density is used to evaluate the heat stored in this layer in a similar way to Polyakov et al. (2011), where the heat content derived for this upper portion of the water column is divided by the depth over which it is computed. This is equivalent to an average temperature over that depth range.

## 3 The Atlantic Water core across the Arctic

Investigating how the AW core changes across the Arctic Ocean can give a good picture of the behaviour of the AW layer in general. Figure 2 shows maps of the potential temperature, salinity, pressure and potential density of the AW core from all observations, giving an idea of the general spatial distribution of the core properties.

Figure 2b highlights the temperature difference between the AW core in the Eurasian Basin and western Arctic. The core loses heat as it is advected around the basin - its temperature in the Canada Basin is approximately 1.5°C lower than where it is first subducted under the fresh surface layer at the southern boundary of the Eurasian Basin. The most significant heat loss is seen here, where, much like in the Nordic Seas (Lind et al., 2018), the AW loses heat to the atmosphere and though mixing with the cooler surface layer. This also freshens the AW (Figure 2c). The higher AW core temperature

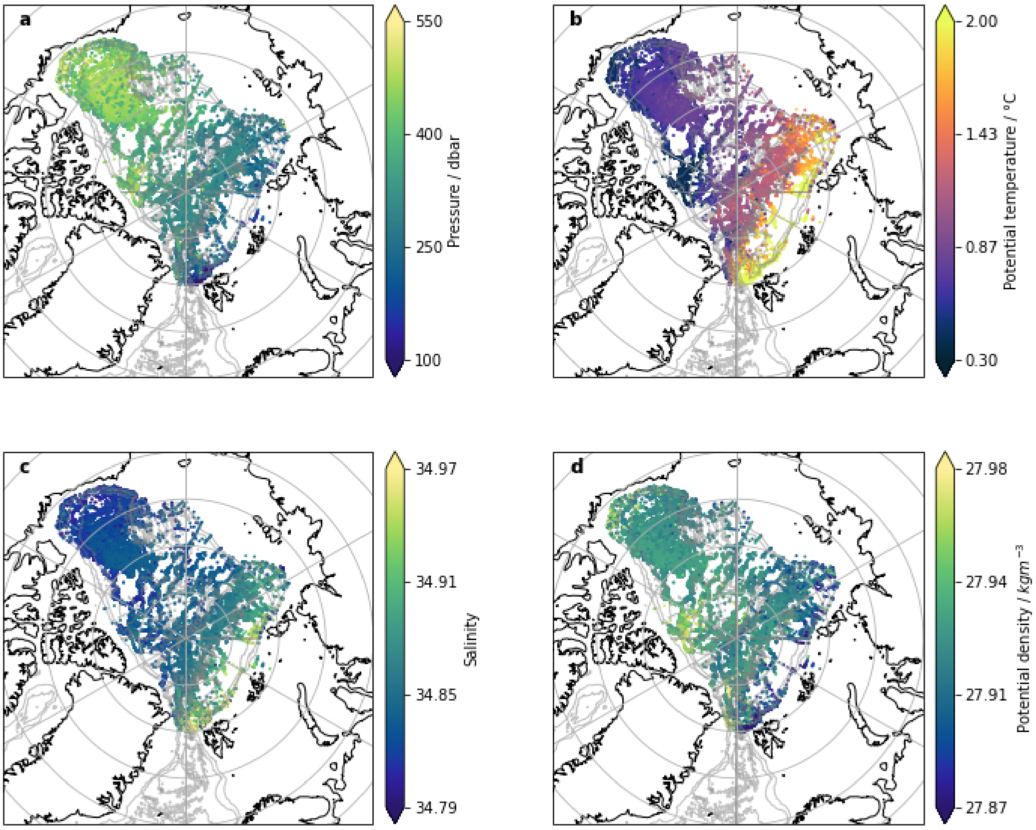


**Figure 2.** Maps showing (a) pressure (b) potential temperature (c) salinity and (d) potential density of all AW core data points used in this study.

along the Lomonosov Ridge relative to the western Arctic boundary suggests that the AW that recirculates back along the ridge is warmer than that which continues towards the western Arctic.

The salinity of the core (Figure 2c) decreases on its journey around the Arctic, particularly in the Eurasian Basin where it mixes with fresher surface waters upon subduction. Turbulent mixing may play an important role in AW freshening in parts of the western Arctic - the difference in AW core salinity (and temperature) between the boundary and interior of the Canada Basin is indicative of this. Whereas the AW in the interior of the Canada Basin has travelled around the north of the Chukchi Plateau, the AW at the boundary has travelled over the Chuckchi Plateau's complex bathymetry (McLaughlin et al., 2009; Li et al., 2020). The relatively low temperature and salinity of this boundary AW can be explained by enhanced mixing experienced over this rough topography upstream.

Despite the AW core freshening along the AW advection pathway, the density of the core appears to increase from its relatively low value along the southern Eurasian Basin boundary to higher values in the western Arctic and Eurasian Basin interior (Figure 2d). This is surprising given the importance of salinity in governing density at such cold temperatures, and suggests the AW core moves across isopycnals as it is advected around the boundary and spreads into the basin interiors. There are particularly dense, cold regions along the western shelves just north of the Canadian Arctic Archipelago (CAA) and Greenland, which suggest that cold, dense shelf flows from sea-ice formation on the shelves are mixing with the AW layer here. This interaction between AW and dense water cascading from shelves has been reported in both the eastern and western Arctic (Ivanov & Golovin, 2007; ?, ?) and could play a key role in the evolution of AW core temperature and density along the AW advection pathway.

The AW core depth exhibits a bimodal structure, as shown in Figure 2a, being much deeper in the Canada Basin (approx. 500 m) than the Eurasian Basin (approx. 300 m) due to the Ekman pumping associated with the winds which drive the Beaufort Gyre. The effect of the Beaufort Gyre on the AW in the Canada Basin can also be seen in the (un-smoothed) vertical temperature profiles in Figure 3, where the cool waters of the gyre suppress the AW layer to a much greater depth than that at which it resides in the eastern Arctic. However, the important role that the halocline plays in isolating the AW from the surface can be observed across the whole Arctic (Figure 3).

Zig-zags/staircase features in these un-smoothed profiles also indicate the presence of thermohaline intrusions which form in the presence of temperature and salinity gradients along isopycnals (Ruddick, 1992), and are an important mechanism for AW transport from the boundary to the interior of both the Canada and Eurasian Basins (McLaughlin et al., 2009; Kuzmina et al., 2011). These intrusion signatures are seen in data throughout the 21$^{\mathrm{st}}$ century in the Canada Basin. Intrusions are also seen in the Eurasian Basin throughout the time period covered in this study, providing strong evidence for their long-term presence in this region, although they have been seldom documented beyond the Canadian Basin in previous studies.

## 4 Regional differences in Atlantic Water properties and their temporal variability

Although the maps in Figure 2 give an idea of the general spatial variability of AW, they do not indicate how the AW may have changed over the time period studied. This section will explore the temporal variability observed in the AW layer in different regions of the Arctic. The potential temperature profiles in Figure 3 are coloured by the year in which they were taken, and demonstrate the notable interannual variability in temperature exhibited in the water column throughout the Arctic Ocean.

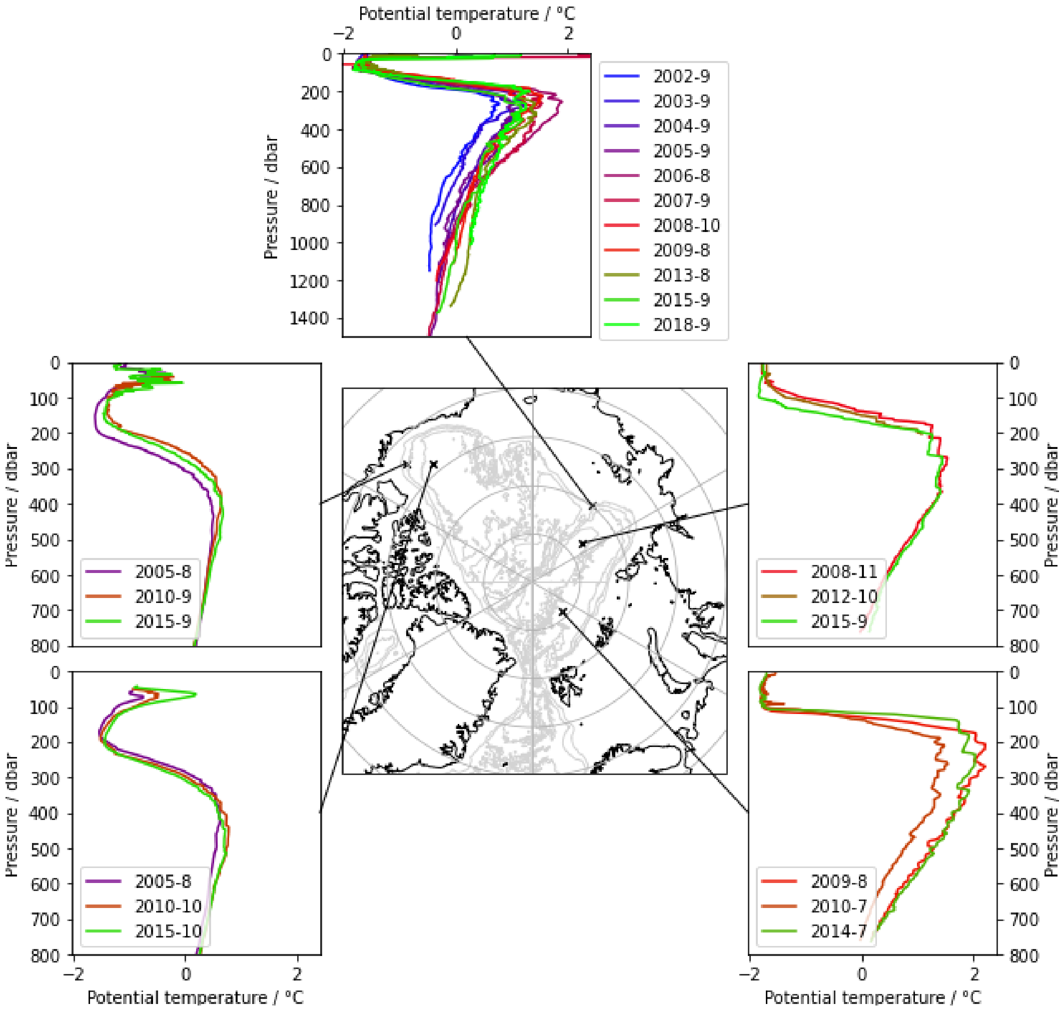


**Figure 3.** Un-smoothed potential temperature profiles at various locations across the Arctic Basin. Profiles are coloured by the year in which they were taken, with year and month given in the legend. Note the change in y-axis scale in the uppermost plot.

The uppermost plot in Figure 3 uses profiles from moorings at the eastern Lomonosov Ridge, sampling the AW boundary current. The depth range sampled by the moorings captures both AW branches - the Fram Strait Branch Water (FSBW) and the Barents Sea Branch Water (BSBW), centered at around 200-500 m and 750-1000 m, respectively. The temperature of these two branches here appears to vary independently in time. The BSBW warms consistently throughout the period sampled, hinting at a more systematic change in BSBW temperature, which could be explained by surface air temperature increases over the Barents Sea (Skagseth et al., 2020) or reductions in sea-ice import to the region (Lind et al., 2018). The FSBW temperature is more variable, reflecting the variability of AW inflow temperature through the Fram Strait (Ivanov et al., 2012). The heat loss experienced by the AW in the Barents Sea may act as a buffer for BSBW against high-frequency variation in upstream AW temperature.

Building on the regional differences in AW shown in Figure 2, Figures 4-7 highlight how the properties of the AW core in the eastern (blue) and western (red) Arctic evolve with time. Maps and annual normalised histograms show how the temperature, salinity, density and pressure of the AW core change. The period covered by each map is indicated by grey lines enveloping the corresponding annual histograms - these periods were chosen to account for the varying amount of data available during each period. The reader is referred to Figure 1 for time series of the amount of data available from each region.

The year-to-year spatial variation in data distribution in the eastern Arctic makes inferring any trends from the histograms for the eastern Arctic difficult, and no significant trend can be found. However, the more consistent spatial distribution of data in the western Arctic and lack of spatial sampling bias in the mooring data (shown in black) allow trends to be inferred for the Canada Basin. The differences in the range of temperature and salinity data between the east and west highlights the transformation undergone by the AW as it travels around the basin, reinforcing what was shown in Figure 2, with AW core salinity and temperature decreasing due to mixing, and AW core density increasing as it moves across isopycnals. AW core trends in the west oppose those expected from the Atlantification reported in the east, despite the advective link between AW in the two regions.

The mooring data in the histograms of Figure 4 reveal a gradual cooling of 0.5°C in the Canada Basin after 2002, presumably after the arrival of the AW core warm temperature anomaly which entered the Canada Basin in the early 2000s (after having entered the Arctic through the Fram Strait in 1990, McLaughlin et al. (2009); Li et al. (2020)). The maps in Figure 4 show the spread of this anomaly from the northern edge of the Chukchi Plateau into the interior of the Canada Basin in 2000–2004, with a more homogeneous AW core temperature field in 2005–2009.

The histograms in Figure 5 and Figure 6 show an increase in AW core salinity and density in the Canada Basin throughout the mooring time period (2003–2018). Enhanced interaction between AW and dense shelf flows upstream in the AW boundary current could explain this salinity increase, reducing the relative freshness of the core in the west compared to the east. The maps show that the AW core at the Canada Basin boundary is more dense pre-2000 than post-2000, so this variation in density could be part of a longer-term oscillation. However, enhanced brine rejection from winter sea-ice formation due to reduced Arctic summer sea-ice area could be causing more dense, saline shelf flows to interact with AW, and raises the possibility that the Canada Basin AW core salinity increase is part of a forced long term trend. No trend was found in the mean salinity of the AW layer in this region, however; the trend is only apparent at the AW core depth. This could be due to a freshening of the upper AW layer associated with other factors such as increased ventilation upstream (Pérez-Hernández et al., 2019) counteracting the increase in salinity seen at the core depth.

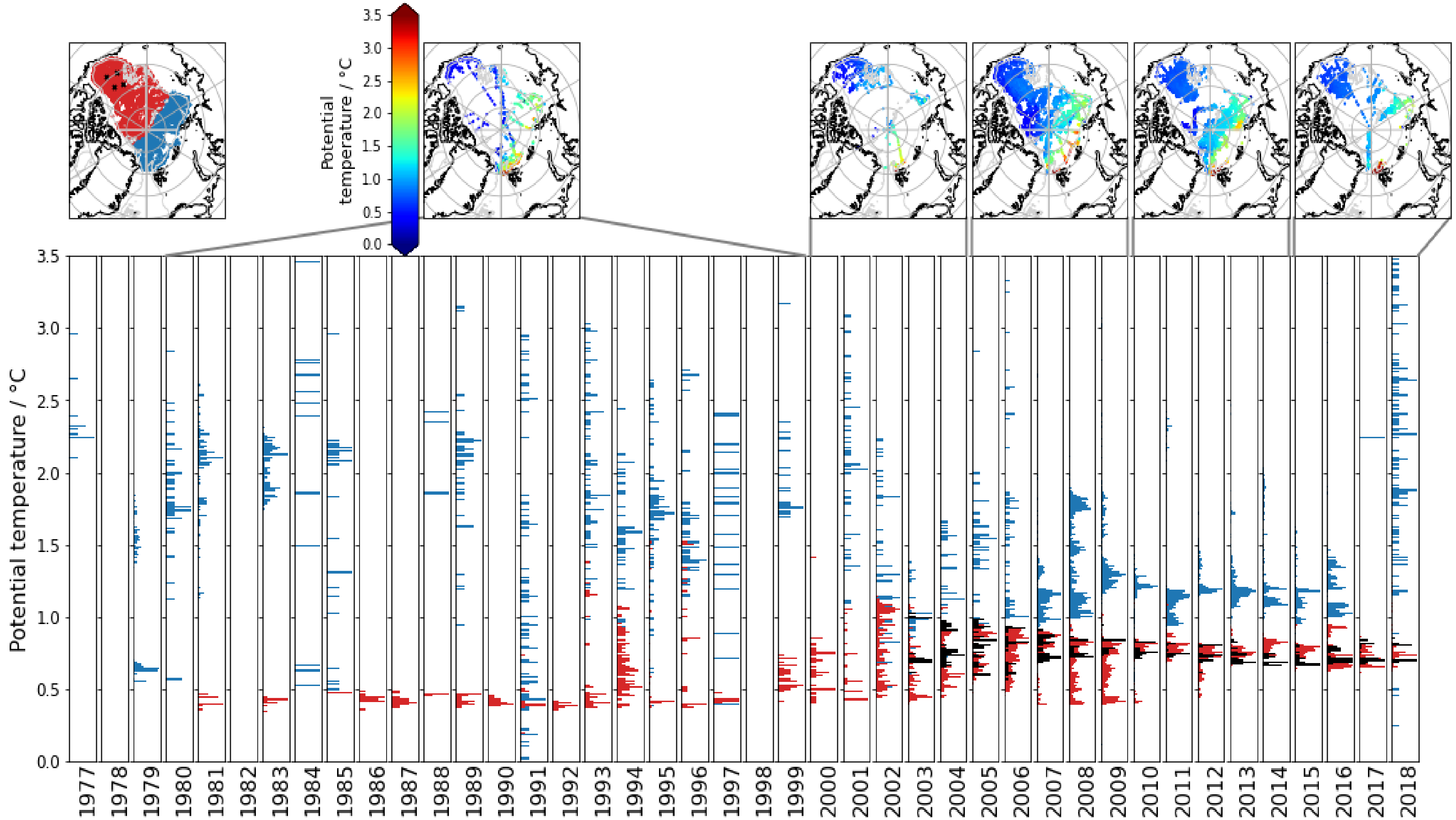


**Figure 4.** Annual normalised histograms of AW core potential temperature. Histogram data is coloured by region, with blue for eastern data, red for western data, and black for western mooring data - as shown in the map at the top left. The five maps to the right show the spatial distribution of the data in the histograms contained within each pair of grey lines.

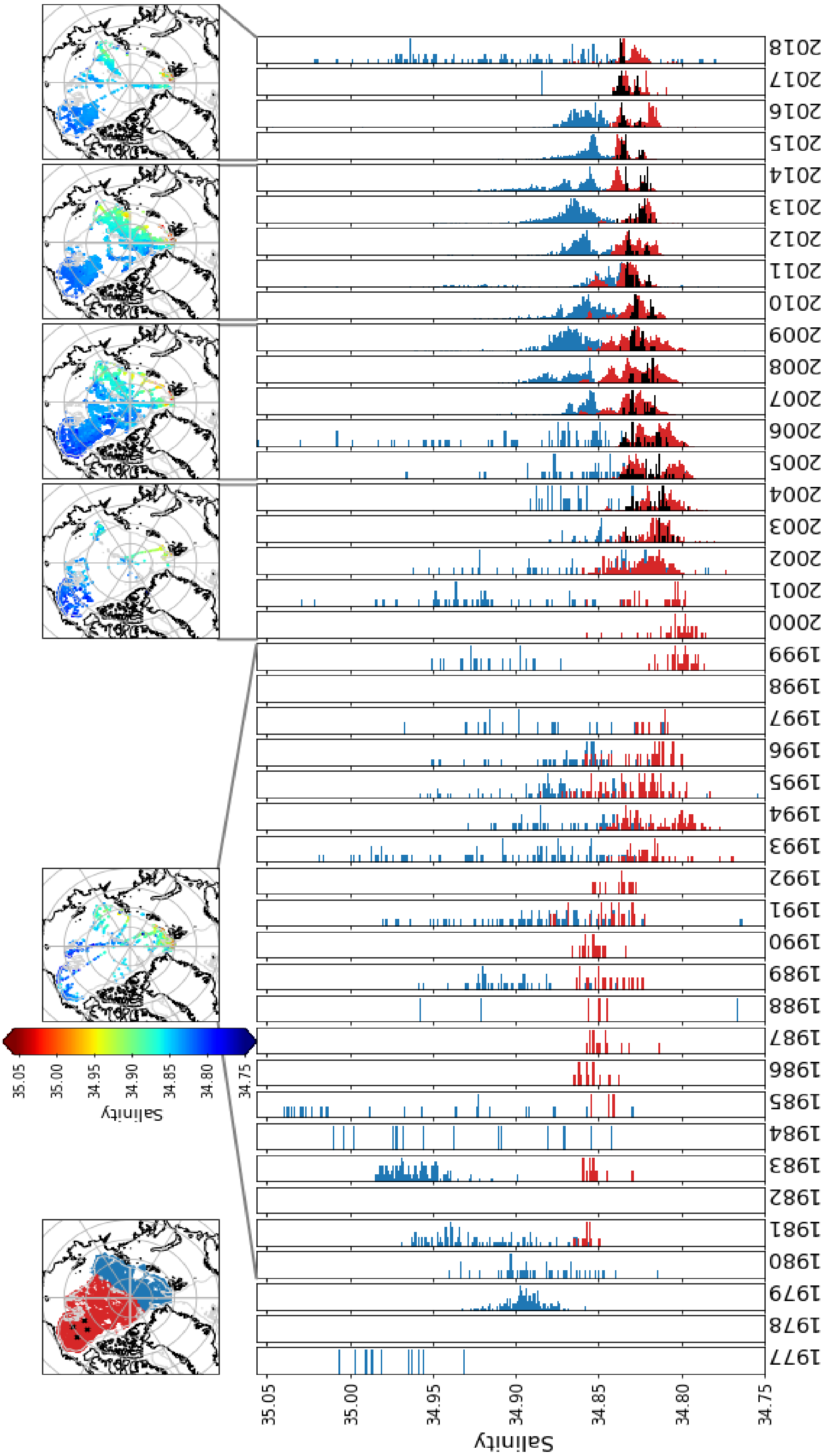


**Figure 5.** As Figure 4 for AW core salinity .

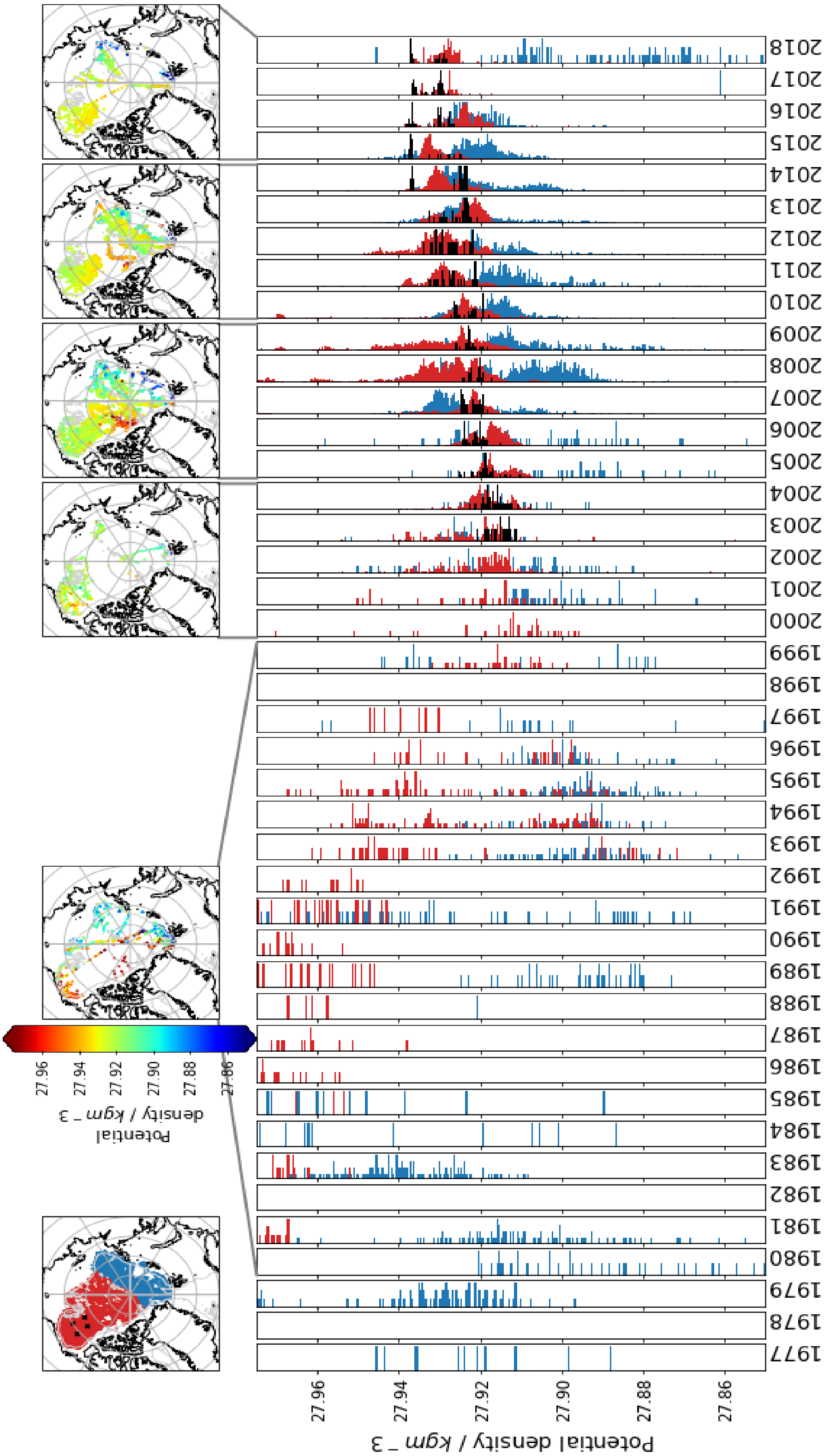


**Figure 6.** As Figure 4 for AW core potential density .

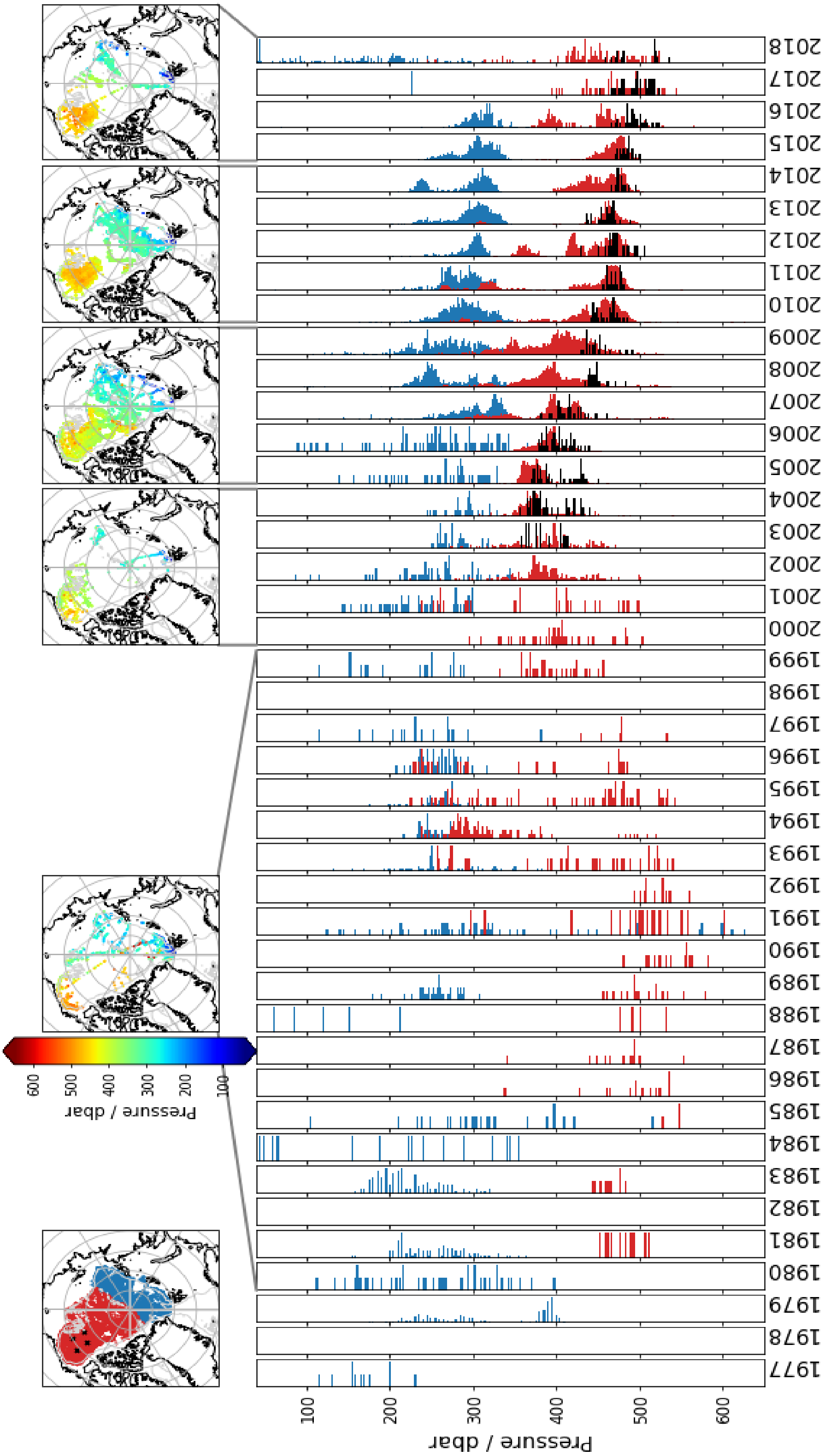


**Figure 7.** As Figure 4 for AW core pressure
.

The most prominent trend in the histogram figures is that of the Canada Basin mooring data in Figure 7, which show a deepening of the AW core. Zhong and Zhao (2014) showed that the AW deepening caused by the spin up of the Beaufort Gyre dominates over the influence of AW core density on depth if the gyre intensifies sufficiently, with AW position in relation to the gyre centre becoming more important than its density from 2007 onwards. This means that when the gyre is sufficiently intense, AW suppressed by the gyre can reside deeper than other AW that is denser (e.g. that at the Canada Basin boundary which the gyre does not suppress). The histograms in Figure 7 show that the deepening of the AW core coincides with the isopycnal deepening reported by Zhong and Zhao (2014) and others. However, the histograms show continued AW core deepening despite the gyre stabilisation after 2008 (Zhang et al., 2016). Based on this figure we speculate that a combination of gyre intensification and AW core salinity/density increase caused a deepening of the AW core up to 2008, with the latter continuing the deepening in subsequent years.

## 5 AW variability at transects and moorings

Broad regional trends in AW core properties have been discussed above. To investigate these further, and put AW core changes within the context of the wider water column, the temporal variability of data at moorings and across regularly repeated CTD transects is investigated below. This should reveal more about the implications of the AW changes for water column stratification and heat distribution.

### 5.1 Eurasian Basin

The potential temperature and salinity along a NABOS CTD transect repeated from 2002–2018 across the AW boundary current in the eastern Eurasian Basin is shown in Figure 8. The year of each transect is given in the plot, and the AW core depth is identified with a black dot. The vertical black lines near the surface of the transects show the location of the CTD profiles. Data between these profiles have been interpolated using a Delaunay triangulation grid. The AW layer warms throughout the time period, but the warming is pulse-like rather than continuous, with one warm pulse peaking in 2007–08 (likely the same warm pulse of AW that entered through Fram Strait around the year 2000 (Polyakov et al., 2005, 2011)) and a second in the 2018 section. The AW core in 2018 is 1°C warmer than that in 2002. The salinity of the AW also shows an increasing trend throughout the time period covered in Figure 8, although regions and years of high salinity are not coincident with regions or years of high temperature.

Figure 9 allows for a more quantitative assessment of the changes in the water column at this location. The first three panels of this figure show the evolution of AW core properties across the transect. This figure shows more clearly that the core freshens onshore in most years, suggesting that AW is mixing with fresher waters from the shelf or that the AW that reaches the shelf is that which is fresher. As above, the core temperature (and AW layer heat content shown in panel five) exhibits warm pulses which are superimposed upon a general warming trend across the period. Notably the heat content of the AW layer increases to three times its 2002 value in 2018. The salinity and depth of these pulses differ, however - the AW core during the warm pulse in 2018 is fresher and shallower than the one in 2008. A weakened halocline may have allowed the warm AW to shoal higher in the water column and mix with the fresher surface layer, as reported by Polyakov, Rippeth, et al. (2020). The 2013 transect, although slightly cooler than those from 2008 and 2018, has a comparatively salty, deep AW core. This non-coincidence of AW core salinity and temperature changes suggests that even enhanced mixing due to a weaker halocline does not mask the signal of these warm AW pulses.

The fourth panel of Figure 9 shows the “heat content density” (the heat content of a portion of the water column divided by the height over which it is computed) of the

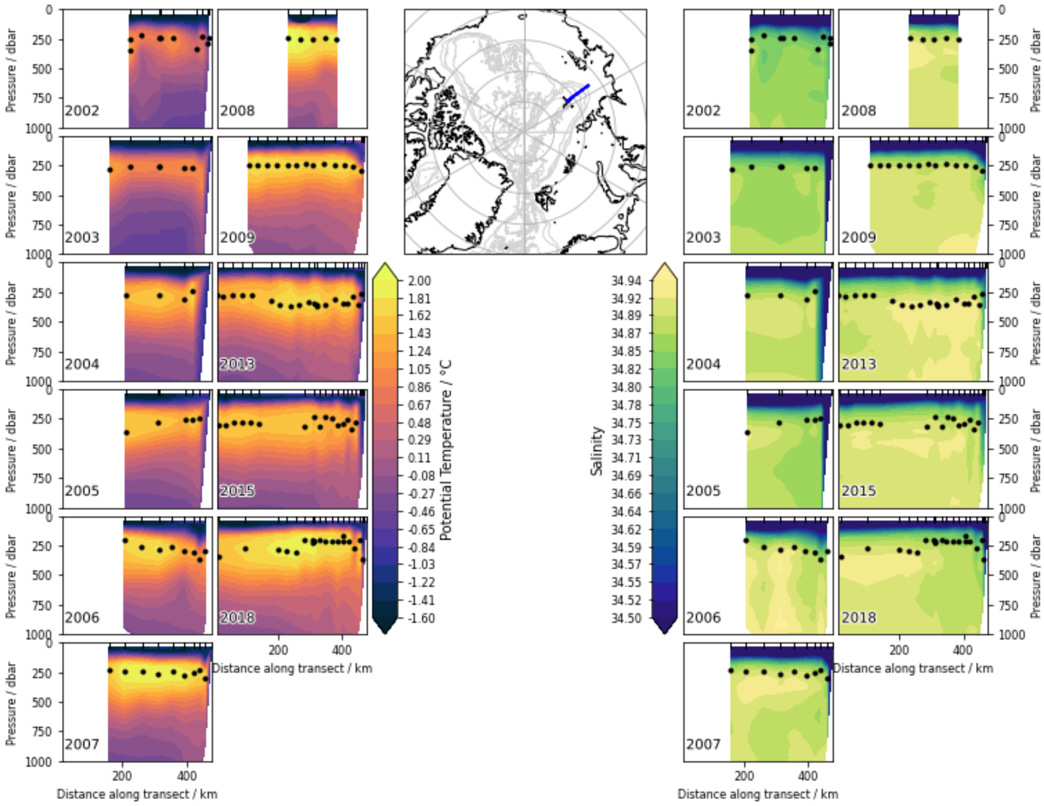


**Figure 8.** Potential temperature and salinity along a repeated CTD transect in the eastern Eurasian Basin. In all years, transects were measured in August, September or October. The origin of the x-axis of the transect is marked with a black cross on the map. CTD profile locations are marked on the transect plots with vertical black lines at the surface. The black dots on the transect plots denote the location of the AW core, and the year in which each transect was taken is given at the bottom left of each plot.

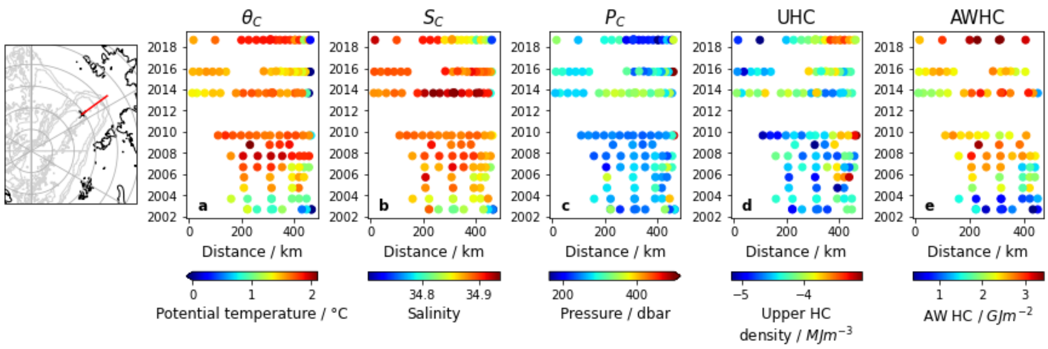


**Figure 9.** Water column properties across a repeated CTD transect in the eastern Eurasian Basin. Transect location is shown on the map, with a black cross denoting the x-axis origin of the transect plots. Transect plots show (a) AW core potential temperature, (b) AW core salinity, (c) AW core pressure, (d) heat content density of the water column above the AW layer, denoted as upper heat content (UHC), and (e) total heat content of the AW layer.

sampled water column above the AW layer, denoted as upper heat content (UHC) in the figure. This is essentially a measure of the average temperature of the surface layer and halocline. UHC increases when the AW core salinity is low and AW core depth is shallow - perhaps an indication that a shallower AW layer transfers more heat to the halocline and surface layer. Despite the similarities in AW core temperature of the 2009 and 2013 transects, the fresher/shallower core in 2009 coincides with a larger surface layer heat content density. The strength of the halocline plays an important role in governing AW salinity, and this figure further emphasises the importance of the Eurasian Basin halocline in governing the extent of Atlantification in the eastern Arctic, regardless of the temperature of AW itself. This is also highlighted in recent work by Polyakov et al. (2018), where halocline stability, quantified using density anomalies throughout the layer, is identified as a key climate change indicator in the region. The implication that AW shoaling is more influential than AW temperature change on surface layer heat content is not surprising given the low levels of vertical mixing throughout the Arctic (Fer, 2009). This is also reflected in the dissimilarity between variations in AW layer heat content and UHC seen in Figure 9.

### 5.2 Canada Basin

Figure 10 shows the same analysis applied to two repeated CTD transects in the Canada Basin. This allows for detection and comparison of any signals advected downstream from the Eurasian Basin transect in Figure 9. The length of the transects also enables comparisons between AW found on the boundary and within the interior of the Canada Basin.

As in the Eurasian Basin, Figure 10 shows evidence of the pulse-like nature of AW core temperature evolution, with warm AW core values in the interior in the mid-2000s indicative of the warm anomaly that arrived in the Canada Basin in the early 2000s (McLaughlin et al., 2009). As seen in Figure 2, AW at the Canada Basin boundary (>1000 km along section A, and the furthest few data points of section B) is cooler and fresher than that in the interior due to the enhanced mixing it experiences upstream over the rough bathymetry of the Chukchi Plateau (McLaughlin et al., 2009; Li et al., 2020). This enhanced mixing and cooling is the likely reason why the warm temperature anomaly is not seen at the boundary in Figure 10 - the temperature signal is much weaker there than it is in the interior.

On both transects, at the boundary, AW core temperature and salinity vary similarly, presumably because both of these properties are governed by the same mixing processes upstream. This is not the case in the interior, however, where from 2012 onwards both transects see an increase in AW core salinity which is not reflected in the temperature. This could be related to the thermohaline intrusions through which the AW enters the interior from the Chukchi Plateau, with the heat diffusing away from these intrusions quicker than the salt, leaving a saline core with no warm temperature signal. This is also indicated by the AW layer heat content, which remains high in the interior of section B after the AW core has cooled. The AW core salinity increase (which is also seen at the boundary and in Figure 5) could be related to enhanced AW mixing with dense, saline flows from sea-ice formation on the shelves near the Canada Basin. Flux of dense water cascading from these shelves is indeed increasing, as reported recently by Luneva et al. (2020).

The slight warming of the AW core temperature in the interior of section B of Figure 10 in 2016 could be evidence of the AW warm anomaly observed upstream of the Chukchi Borderlands in 2010 (after having entered the Arctic Ocean through the Fram Strait in the 2000, Li et al. (2020)). It can also be seen at the Eurasian Basin transect in Figure 9 around 2008, and until now has not been conclusively observed in the Canada Basin interior. This gives AW advection timescales from the eastern Eurasian Basin to the north

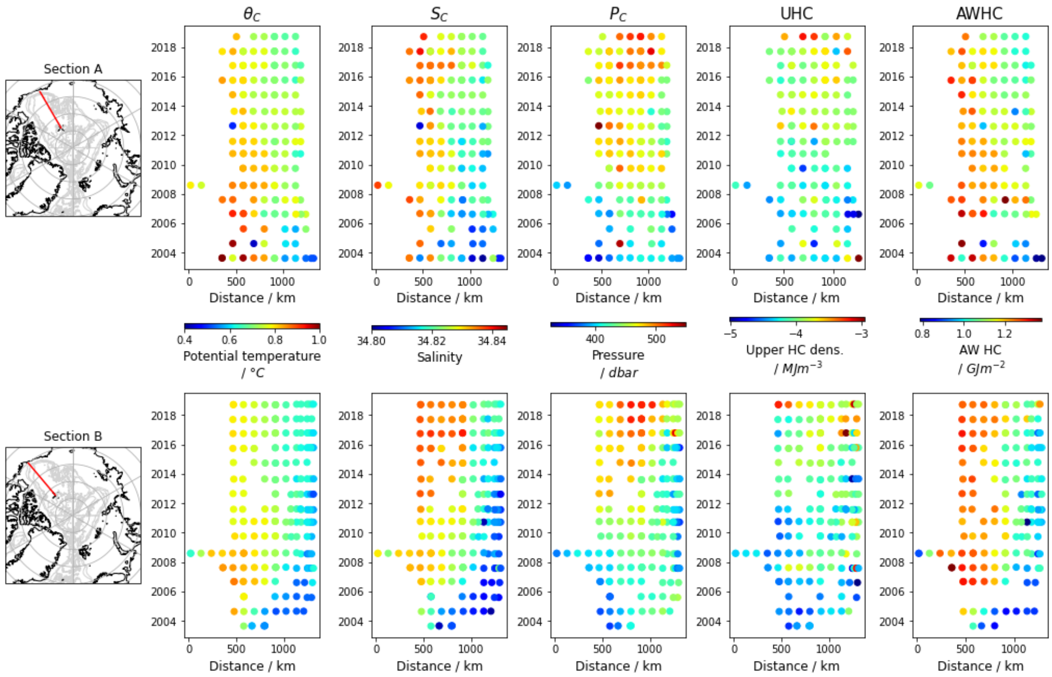


**Figure 10.** Water column properties across two repeated CTD transects in the Canada Basin. Transect location is shown on the maps, with black crosses denoting the x-axis origin of each transect. Remaining panels show (a) AW core potential temperature, (b) AW core salinity, (c) AW core pressure, (d) heat content density of the water column above the AW layer, and (e) total heat content of the AW layer.

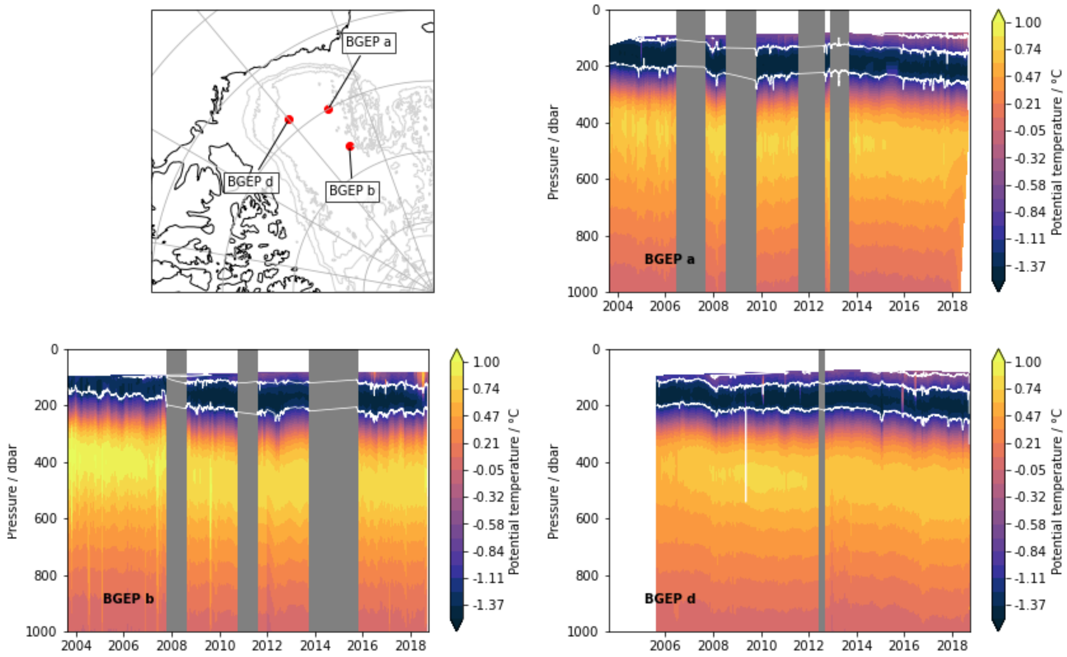


**Figure 11.** Hovmöller plots of potential temperature from three moorings in the Canada Basin (BGEP moorings a, b and d - locations shown on map). White lines denote the isopycnals - the deepest at 27 $kgm^{-3}$, contour interval 1 $kgm^{-3}$. Grey regions cover time periods with insufficient data.

of the Chuckchi Borderlands, and around the north of the Borderlands into the Canada Basin interior of order 8 years, in agreement with other observational studies (Polyakov et al., 2011; Li et al., 2020). The amplitude of the warming is low compared to that of the previous warm temperature anomaly - despite the second anomaly being 0.24°C warmer than the first in the Eurasian Basin (Polyakov et al., 2010). This could be due to enhanced heat loss experienced by the AW during its advection, associated with increased ventilation and/or interaction with shelf flows. Further observational data would be needed to confirm the presence of this second AW warm anomaly in the Canada Basin interior, however.

Figure 7 showed that the depth of the AW core in the Canada Basin increases throughout the time period covered. Comparing the patterns of change in AW core depth and salinity in Figure 10 suggests that the salinity increase is not the most important driver of the depth increase. As discussed, the spin-up of the Beaufort Gyre and associated enhanced downwelling influences AW depth (Lique & Johnson, 2015; Lique et al., 2015; Zhong & Zhao, 2014), so the increase in core depth could be explained by gyre intensification (which continued at least until 2008, Zhang et al. (2016); Regan et al. (2019)).

Figure 10 shows a further increase in AW core depth after 2008, however, along with a general increase in surface layer heat content density. The Hovmöller plots in Figure 11 reveal more about the mechanisms behind the AW core deepening in the Canada Basin beyond 2008, and also help explain this increase in upper layer heat content density. This figure shows Hovmöller plots of potential temperature profiles from three of the BGEP moorings in the Canada Basin (mooring c having been omitted due to the shorter time-series available there), with white lines marking isopycnal depths. The core depth varies in concert with isopycnal depth at all moorings, again emphasising that changes elsewhere in the water column, rather than those of the AW properties themselves, are likely driving AW depth changes here. With the exception of mooring d (which the gyre moved away from during the start of the period shown (Regan et al., 2019)), the isopycnals and hence AW deepened up until 2008, as the gyre intensified and stabilised (Zhang et al., 2016). The subsequent deepening of the AW can be attributed to the appearance of a warm, fresh water mass near the surface. This is likely to be Pacific Water which penetrated the Canada Basin halocline in the early 2010s (Timmermans et al., 2014). Therefore, both the gyre intensity and presence of Pacific Water in the halocline appear to be the main factors behind AW core depth increase in the Canada Basin. The increase in AW core density does not appear to play an important role, as seen in Figure 10. The increase in upper layer heat content density seen in Figure 10 can be attributed to the presence of this Pacific Water, and does not coincide with a change in AW layer heat content (shown in the final panel of Figure 10). This suggests that increases in sea-ice bottom-melt reported in the Beaufort Sea (Perovich & Richter-Menge, 2015) are likely due to Pacific Water (along with other local features such as the near-surface temperature maxima (Jackson et al., 2012; Timmermans, 2015)), not Atlantic Water heat. The deepening of the AW and its increased isolation from the surface in the Canada Basin is in stark contrast to the concurrent Atlantification seen in the Eurasian Basin.

## 6 Relationships between properties of the AW core and the rest of the AW layer

Much of the analysis in this study has involved the use of the AW core to infer properties of the AW within the Arctic. It is therefore important to investigate how representative properties of the AW core are of the AW layer in general. In section B of Figure 10, for example, there was a suggestion that diffusion of heat away from the AW core within thermohaline intrusions caused a decrease in AW core temperature, while total AW layer heat content remained stable. In this subsection, general relationships between AW core properties and integrated AW layer properties will be explored.

The maps in Figure 12 show total AW layer heat content during different time periods, chosen to give a roughly even data distribution between panels. As most observational profiles do not sample deep enough to cover the entire AW layer, there are substantially less AW heat content data (1500 data points) than AW core data. This, of itself, emphasizes the usefulness of the AW core in assessing the pathways and evolution of the AW layer.

In the Canada Basin, AW heat content increased in the mid-2000s (Figure 12, panels b to c) after the arrival of the AW warm anomaly (McLaughlin et al., 2009; Li et al., 2020) and has since remained at that higher level of approximately $1.5{\times}10^9\ Jm^{-2}$, with no long term trend observed. The eastern Eurasian Basin saw an increase in AW heat content throughout the period studied, in-line with the reported Atlantification of the region (Lind et al., 2018; Polyakov et al., 2010, 2017). Figure 12 shows a stark difference between AW heat content in the Eurasian and Canada Basins, implying that the AW that bifurcates and recirculates towards the Fram Strait along the Lomonosov Ridge is warmer than the AW in much of the western Arctic. The heat content maps in Figure 12 are very similar to the AW core potential temperature maps in Figure 2, further suggesting that the AW core temperature captures AW heat content variability well in both time and space.

To be more quantitative in this conclusion, correlations between AW core temperature and AW heat content were computed. Figure 13 shows scatter plots between pairs of variables computed from profiles in both the eastern and western Arctic (these regions are defined in Figure 1). R-squared values for each of the plots are given, along with regression lines. The relationship between total AW heat content and the potential temperature of the AW core is shown in Figure 13a. There is a strong correlation between these two variables in both the eastern and western Arctic, highlighting the general ef-

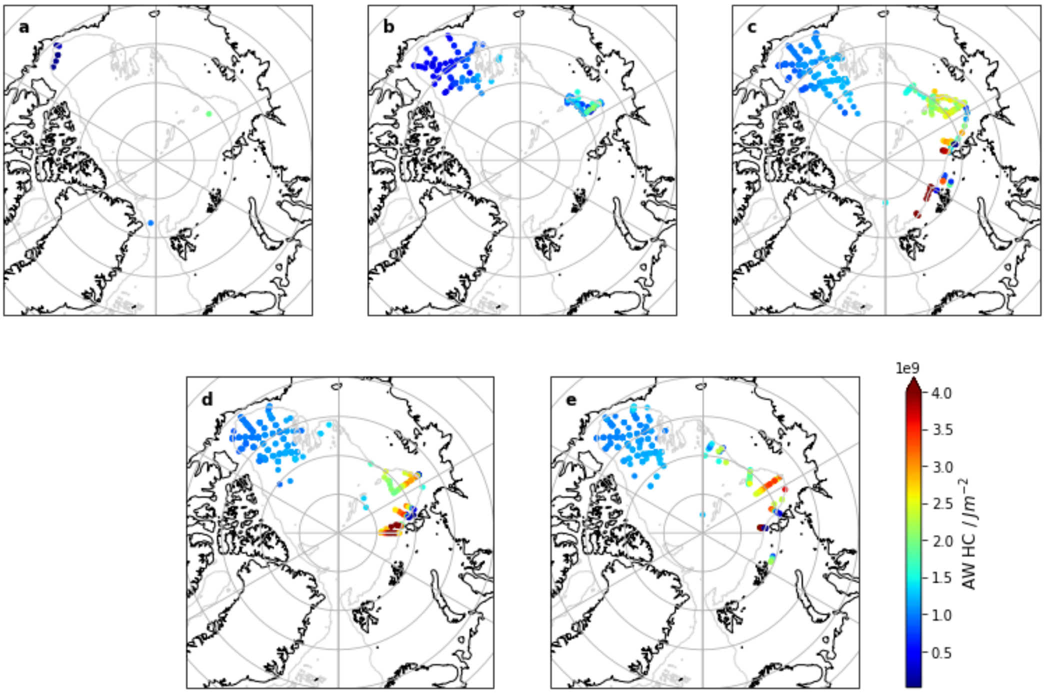


**Figure 12.** Maps of total AW layer heat content from all profiles which sampled the entire AW layer (defined as the layer between the two 0 °C crossing points either side of the AW core) for (a) 1980-1999, (b) 2000-2004, (c) 2005-2009, (d) 2010-2014, and (e) 2015-2018.

fectiveness of the AW core temperature as an easily measurable metric for assessing AW heat content. However, the correlation is not as high as perhaps would be expected - likely owing to the diffusion of heat away from intrusions as mentioned above - and differs between eastern and western basins.

Figures 13b and 13c show correlations between other properties of the AW core and AW layer. Figure 13b shows the relationship between AW core depth and the depth of the upper boundary of the AW layer (i.e. the 0°C crossing point above the AW core). Although there is a strong correlation in the western Arctic, this is not the case in the east - likely due to mixing between the upper AW and the fresher, cooler surface and halocline waters. This highlights the care that should be taken when using AW core depth to assess AW layer shoaling here.

Comparing the mean salinity of the AW layer with the AW layer heat content can give an idea of the role that mixing with fresher waters plays in AW heat loss. Figure 13c shows that, while there is a relatively high correlation between these variables in the east, the correlation is negligible in the west. This implies that although mixing with fresher waters is important for AW heat loss in the Eurasian Basin - as would be expected given that the AW subducts beneath the cooler, fresh polar waters here, losing a lot of heat - it is not as important in the western Arctic. As seen above, heat loss in the majority of the western Arctic may be more affected by mixing with cold dense flows from brine rejection at the shelves than mixing with fresher waters sitting above the strong halocline.

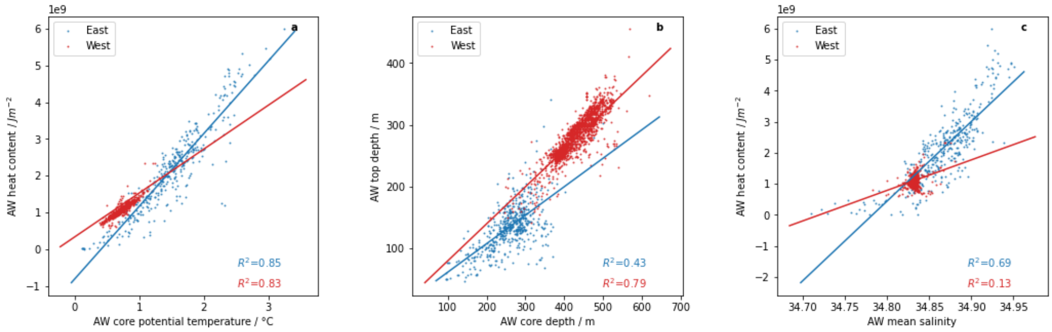


**Figure 13.** Scatter plots between (a) AW core potential temperature and total AW heat content, (b) AW core depth and AW upper depth, and (c) AW mean salinity and total AW heat content. Blue data is from the eastern Arctic (defined in Figure 1), with red data from the western Arctic. R-squared values and regression lines are shown for each scatter plot.

## 7 Conclusion

This study has used hydrographic profiles from across the Arctic from the 1970s to 2018 to build a picture of AW in the Arctic Ocean entirely from observations, and investigate its spatial and temporal variability. Much of the analysis has focused on the AW core (the depth at which the maximum potential temperature occurs). This was found to be a generally effective and easily detected metric to assess the heat content of the AW layer. However, the depth of the AW core is not always reflective of the depth of the top of the AW layer, particularly in the eastern Arctic.

In general, as the AW is advected around the Arctic the potential temperature and salinity of its core decrease. Despite this freshening, the AW core density increases along its advection pathway as it moves across isopycnals within the AW layer. We found evidence of interaction between the AW and cold, saline flows from the shelves, which may be an important mechanism through which the AW loses heat upon advection around the Arctic - particularly in the west (with heat loss to the atmosphere and fresh surface waters more important in the east). The increase in AW core density and salinity in the western Arctic from 2002 onwards indicates that this interaction may be increasing, perhaps due to enhanced winter sea-ice formation as summer sea-ice extent reduces. No such trend in mean AW layer salinity was found, however.

The evolution of AW differed between the eastern and western basins of the Arctic. East of the Lomonosov Ridge, in the Eurasian Basin, AW temperature and AW heat content increased from 2002–2018 with warm pulses superimposed upon this trend. In contrast to this, and the widely reported Atlantification in the east, the western Arctic saw AW core temperatures decrease and AW heat become more isolated from the surface. This was due to Beaufort Gyre intensification and an influx of warm Pacific Water, both of which deepened the halocline. These findings suggest a future Atlantic regime and Pacific regime in the Arctic, separated by the Lomonosov Ridge - with AW affecting sea-ice in the east, and Pacific Water influencing sea-ice in the west. This contrasting regional evolution is in agreement with other recent studies, which describe halocline weakening, AW shoaling, and increased sub-Arctic influence in the Eurasian Basin, contrasting with a freshening and deepening of the surface layer in the Amerasian Basin driven by local atmospheric conditions (Polyakov, Rippeth, et al., 2020; Polyakov, Alkire, et al., 2020).

Despite the limitation of sparse, temporally inhomogeneous oceanographic measurements in the Arctic, pan-Arctic observational analysis can give useful insights into the overall temporal and spatial patterns of heat distribution in the Arctic Ocean. Given the challenges of realistically representing the AW layer in forced ocean-sea-ice and coupled climate models, and the stark regional differences emerging in the Arctic Ocean, the use of pan-Arctic observations for model validation and benchmarking will be essential. Only by combining insight from observations and models will we be able to accurately determine what the future Arctic will look like under a changing climate, which is important both for the region itself as well as for the wider climate system.

## Acknowledgments

This study was funded by the Natural Environment Research Council (NERC) via a DTP studentship under grant number NE/L002612/1. Data used in this study are available from `http://www.whoi.edu/itp` (for ITP data), `https://www.whoi.edu/beaufortgyre` (for BGEP data), `https://uaf-iarc.org/nabos` (for NABOS data), and `https://www.nodc.noaa.gov/OC5/WOD/pr\_wod.html` (for WOD data).

## References

Aksenov, Y., Ivanov, V. V., Nurser, A. J. G., Bacon, S., Polyakov, I. V., Coward, A. C., ... Beszczynska-Moeller, A. (2011). The arctic circumpolar boundary current. *J. Geophys. Res. Ocean.*, *116*(9). doi: 10.1029/2010JC006637

Anderson, L. G., Bjrrk, G., Jones, E. P., Kattner, G., Koltermann, K. P., Liljeblad, B., ... Swift, J. (1994). Results from the Oden 91 expedition. , *99*, 3273–3283.

Barton, B. I., Lenn, Y. D., & Lique, C. (2018). Observed atlantification of the Barents Sea causes the Polar Front to limit the expansion of winter sea ice. *J. Phys. Oceanogr.*, *48*(8), 1849–1866. doi: 10.1175/JPO-D-18-0003.1

Beszczynska-Moller, A., Fahrbach, E., Schauer, U., & Hansen, E. (2012). Variability in Atlantic water temperature and transport at the entrance to the Arctic Ocean, 1997–2010. *J. Mar. Sci.*, *69*(5), 852–863. doi: 10.1038/278097a0

Carmack, E., Polyakov, I., Padman, L., Fer, I., Hunke, E., Hutchings, J., ... Winsor, P. (2015). Toward quantifying the increasing role of oceanic heat in sea ice loss in the new arctic. *Bull. Am. Meteorol. Soc.*, *96*(12), 2079–2105. doi: 10.1175/BAMS-D-13-00177.1

Dmitrenko, I. A., Polyakov, I. V., Kirillov, S. A., Timokhov, L. A., Frolov, I. E., Sokolov, V. T., ... Walsh, D. (2008). Toward a warmer Arctic Ocean: Spreading of the early 21st century Atlantic water warm anomaly along the Eurasian basin margins. *J. Geophys. Res. Ocean.*, *113*(5), 1–13. doi: 10.1029/2007JC004158

Fer, I. (2009). Weak Vertical Diffusion Allows Maintenance of Cold Halocline in the Central Arctic. *Atmos. Ocean. Sci. Lett.*, *2*(3), 148–152. doi: 10.1080/16742834.2009.11446789

Ilıcak, M., Drange, H., Wang, Q., Gerdes, R., Aksenov, Y., Bailey, D., ... Yeager, S. G. (2016, apr). An assessment of the Arctic Ocean in a suite of interannual CORE-II simulations. Part III: Hydrography and fluxes. *Ocean Model.*, *100*, 141–161. doi: 10.1016/j.ocemod.2016.02.004

IOC, SCOR, & IAPSO. (2010). *The International Thermodynamic Equation of Seawater-2010: Calculation and Use of Thermodynamic Properties, Manuals Guides.* Paris: UNESCO.

Ivanov, V. V., Alexeev, V. A., Repina, I., Koldunov, N. V., & Smirnov, A. (2012). Tracing atlantic water signature in the arctic sea ice cover east of svalbard. *Adv. Meteorol.*, *2012*. doi: 10.1155/2012/201818

Ivanov, V. V., & Golovin, P. N. (2007). Observations and modeling of dense water cascading from the northwestern Laptev Sea shelf. *J. Geophys. Res. Ocean.*, *112*(9), 1–15. doi: 10.1029/2006JC003882

Jackson, J. M., Williams, W. J., & Carmack, E. C. (2012). Winter sea-ice melt in the Canada Basin, Arctic ocean. *Geophys. Res. Lett.*, *39*(3), 2–7. doi: 10.1029/2011GL050219

Karcher, M., Beszczynska-Möller, A., Kauker, F., Gerdes, R., Heyen, S., Rudels, B., & Schauer, U. (2011). Arctic Ocean warming and its consequences for the Denmark Strait overflow. *J. Geophys. Res. Ocean.*, *116*(2), 1–10. doi: 10.1029/2010JC006265

Karcher, M., Smith, J. N., Kauker, F., Gerdes, R., & Smethie, W. M. (2012). Recent changes in Arctic Ocean circulation revealed by iodine-129 observations and modeling. *J. Geophys. Res. Ocean.*, *117*(8), 1–17. doi: 10.1029/2011JC007513

Karcher, M. J., Gerdes, R., Kauker, F., & Köberle, C. (2003). Arctic warming: Evolution and spreading of the 1990s warm event in the Nordic seas and the Arctic Ocean. *J. Geophys. Res. C Ocean.*, *108*(2), 16–1. doi: 10.1029/2001jc001265

Karcher, M. J., & Oberhuber, J. (2002). Pathways and modification of the upper and intermediate waters of the Arctic Ocean. *J. Geophys. Res.*, *107*(C6), 1–13. doi: 10.1029/2000jc000530

Krishfield, R., Toole, J., Proshutinsky, A., & Timmermans, M. L. (2008). Automated ice-tethered profilers for seawater observations under pack ice in all seasons. *J. Atmos. Ocean. Technol.*, *25*(11), 2091–2105. doi: 10.1175/2008JTECHO587.1

Kuzmina, N., Rudels, B., Zhurbas, V., & Stipa, T. (2011). On the structure and dynamical features of intrusive layering in the Eurasian Basin in the Arctic Ocean. *J. Geophys. Res. Ocean.*, *116*(12), 1–15. doi: 10.1029/2010JC006920

Ladd, C., Mordy, C. W., Salo, S. A., & Stabeno, P. J. (2016). Journal of geophysical research. *J. Geophys. Res. Ocean.*, *121*(8), 5516–5534. doi: 10.1038/175238c0

Li, J., Pickart, R. S., Lin, P., Bahr, F., Arrigo, K. R., Juranek, L., & Yang, X. Y. (2020). The Atlantic Water Boundary Current in the Chukchi Borderland and Southern Canada Basin. *J. Geophys. Res. Ocean.*, *125*(8), 1–20. doi: 10.1029/2020JC016197

Lind, S., Ingvaldsen, R. B., & Furevik, T. (2018, jul). Arctic warming hotspot in the northern Barents Sea linked to declining sea-ice import. *Nat. Clim. Chang.*, *8*(7), 634–639. doi: 10.1038/s41558-018-0205-y

Lique, C., & Johnson, H. L. (2015, nov). Is there any imprint of the wind variability on the Atlantic Water circulation within the Arctic Basin? *Geophys. Res. Lett.*, *42*(22), 9880–9888. doi: 10.1002/2015GL066141

Lique, C., Johnson, H. L., & Davis, P. E. D. (2015, may). On the Interplay between the Circulation in the Surface and the Intermediate Layers of the Arctic Ocean. *J. Phys. Oceanogr.*, *45*(5), 1393–1409. doi: 10.1175/JPO-D-14-0183.1

Lique, C., Johnson, H. L., & Plancherel, Y. (2018). Emergence of deep convection in the Arctic Ocean under a warming climate. *Clim. Dyn.*, *50*(9-10), 3833–3847. doi: 10.1007/s00382-017-3849-9

Lique, C., & Steele, M. (2012, mar). Where can we find a seasonal cycle of the Atlantic water temperature within the Arctic Basin? *J. Geophys. Res. Ocean.*, *117*(C3), n/a–n/a. doi: 10.1029/2011JC007612

Lique, C., Treguier, A. M., Blanke, B., & Grima, N. (2010). On the origins of water masses exported along both sides of Greenland: A Lagrangian model analysis. *J. Geophys. Res. Ocean.*, *115*(5), 1–20. doi: 10.1029/2009JC005316

Luneva, M. V., Ivanov, V. V., Tuzov, F., Aksenov, Y., Harle, J. D., Kelly, S., & Holt, J. T. (2020). Hotspots of Dense Water Cascading in the Arctic Ocean: Implications for the Pacific Water Pathways. *J. Geophys. Res. Ocean.*, *125*(10). doi: 10.1029/2020JC016044

McLaughlin, F. A., Carmack, E. C., Williams, W. J., Zimmermann, S., Shimada, K., & Itoh, M. (2009). Joint effects of boundary currents and thermohaline intrusions on the warming of Atlantic water in the Canada Basin, 1993-2007.

*J. Geophys. Res. Ocean.*, *114*(7). doi: 10.1029/2008JC005001

Pérez-Hernández, M. D., Pickart, R. S., Torres, D. J., Bahr, F., Sundfjord, A., Ingvaldsen, R., ... Pavlov, V. (2019). Structure, Transport, and Seasonality of the Atlantic Water Boundary Current North of Svalbard: Results From a Yearlong Mooring Array. *J. Geophys. Res. Ocean.*, *124*(3), 1679–1698. doi: 10.1029/2018JC014759

Perovich, D. K., & Richter-Menge, J. A. (2015). Regional variability in sea ice melt in a changing Arctic. *Philos. Trans. R. Soc. A Math. Phys. Eng. Sci.*, *373*(2045). doi: 10.1098/rsta.2014.0165

Polyakov, I. V., Alekseev, G. V., Timokhov, L. A., Bhatt, U. S., Colony, R. L., Simmons, H. L., ... Zakharov, V. F. (2004). Variability of the intermediate Atlantic water of the Arctic Ocean over the last 100 years. *J. Clim.*, *17*(23), 4485–4497. doi: 10.1175/JCLI-3224.1

Polyakov, I. V., Alexeev, V. A., Ashik, I. M., Bacon, S., Beszczynska-Möller, A., Carmack, E. C., ... Woodgate, R. (2011). Fate of early 2000s arctic warm water pulse. *Bull. Am. Meteorol. Soc.*, *92*(5), 561–566. doi: 10.1175/2010BAMS2921.1

Polyakov, I. V., Alkire, M. B., Bluhm, B. A., Brown, K. A., Carmack, E. C., Chierici, M., ... Wassmann, P. (2020). Borealization of the Arctic Ocean in Response to Anomalous Advection From Sub-Arctic Seas. *Front. Mar. Sci.*, *7*(July). doi: 10.3389/fmars.2020.00491

Polyakov, I. V., Beszczynska, A., Carmack, E. C., Dmitrenko, I. A., Fahrbach, E., Frolov, I. E., ... Walsh, J. E. (2005). One more step toward a warmer Arctic. *Geophys. Res. Lett.*, *32*(17), 1–4. doi: 10.1029/2005GL023740

Polyakov, I. V., Pnyushkov, A. V., Alkire, M. B., Ashik, I. M., Baumann, T. M., Carmack, E. C., ... Yulin, A. (2017, apr). Greater role for Atlantic inflows on sea-ice loss in the Eurasian Basin of the Arctic Ocean. *Science (80-. ).*, *356*(6335), 285–291. doi: 10.1126/science.aai8204

Polyakov, I. V., Pnyushkov, A. V., & Carmack, E. C. (2018). Stability of the arctic halocline: A new indicator of arctic climate change. *Environ. Res. Lett.*, *13*(12), 125008. doi: 10.1088/1748-9326/aaec1e

Polyakov, I. V., Pnyushkov, A. V., & Timokhov, L. A. (2012, dec). Warming of the Intermediate Atlantic Water of the Arctic Ocean in the 2000s. *J. Clim.*, *25*(23), 8362–8370. doi: 10.1175/JCLI-D-12-00266.1

Polyakov, I. V., Rippeth, T. P., Fer, I., Alkire, M. B., Baumann, T. M., Carmack, E. C., ... Rember, R. (2020). Weakening of cold halocline layer exposes sea ice to oceanic heat in the eastern arctic ocean. *J. Clim.*, *33*(18), 8107–8123. doi: 10.1175/JCLI-D-19-0976.1

Polyakov, I. V., Timokhov, L. A., Alexeev, V. A., Bacon, S., Dmitrenko, I. A., Fortier, L., ... Toole, J. (2010). Arctic ocean warming contributes to reduced polar ice cap. *J. Phys. Oceanogr.*, *40*(12), 2743–2756. doi: 10.1175/2010JPO4339.1

Regan, H. C., Lique, C., & Armitage, T. W. (2019). The Beaufort Gyre Extent, Shape, and Location Between 2003 and 2014 From Satellite Observations. *J. Geophys. Res. Ocean.*, *124*(2), 844–862. doi: 10.1029/2018JC014379

Ruddick, B. (1992). *Intrusive mixing in a Mediterranean salt lens - intrusion slopes and dynamical mechanisms* (Vol. 22) (No. 11). doi: 10.1175/1520-0485(1992)022⟨1274:IMIAMS⟩2.0.CO;2

Rudels, B. (2015). Arctic Ocean circulation, processes and water masses: A description of observations and ideas with focus on the period prior to the International Polar Year 2007-2009. *Prog. Oceanogr.*, *132*, 22–67. doi: 10.1016/j.pocean.2013.11.006

Schauer, U., Loeng, H., Rudels, B., Ozhigin, V. K., & Dieck, W. (2002). Atlantic Water flow through the Barents and Kara Seas. *Deep. Res. Part I Oceanogr. Res. Pap.*, *49*(12), 2281–2298. doi: 10.1016/S0967-0637(02)00125-5

Shu, Q., Wang, Q., Su, J., Li, X., & Qiao, F. (2019). Assessment of the Atlantic water layer in the Arctic Ocean in CMIP5 climate models. *Clim. Dyn.*, *53*(9-10), 5279–5291. doi: 10.1007/s00382-019-04870-6

Skagseth, Ø., Eldevik, T., Årthun, M., Asbjørnsen, H., Lien, V. S., & Smedsrud, L. H. (2020). Reduced efficiency of the Barents Sea cooling machine. *Nat. Clim. Chang.*, *10*(7), 661–666. doi: 10.1038/s41558-020-0772-6

Spielhagen, R. F., Werner, K., Sørensen, S. A., Kandiano, E., Budeus, G., Husum, K., & Marchitto, T. M. (2011). Enhanced Modern Heat Transfer to the Arctic by Warm Atlantic Water. *Science (80-. ).*, *331*(6016), 450–453.

Timmermans, M. L. (2015). The impact of stored solar heat on Arctic sea ice growth. *Geophys. Res. Lett.*, *42*(15), 6399–6406. doi: 10.1002/2015GL064541

Timmermans, M. L., Proshutinsky, A., Golubeva, E., Jackson, J. M., Krishfield, R., McCall, M., … Nishino, S. (2014). Mechanisms of Pacific Summer Water variability in the Arctic's Central Canada Basin. *J. Geophys. Res. Ocean.*, *119*, 7523–7548. doi: 10.1038/175238c0

Toole, J. M., Krishfield, R. A., Timmermans, M. L., & Proshutinsky, A. (2011). The Ice-Tethered profiler: Argo of the Arctic. *Oceanography*, *24*(3), 126–135. doi: 10.5670/oceanog.2011.64

Turner, J. S. (2010, jan). The Melting of Ice in the Arctic Ocean: The Influence of Double-Diffusive Transport of Heat from Below. *J. Phys. Oceanogr.*, *40*(1), 249–256. doi: 10.1175/2009JPO4279.1

Wefing, A. M., Casacuberta, N., Christl, M., Gruber, N., & Smith, J. N. (2020). Circulation timescales of Atlantic Water in the Arctic Ocean determined from anthropogenic radionuclides. *Ocean Sci.*, *17*(1), 111–129. doi: 10.5194/os-17-111-2021

Woodgate, R. A., Aagaard, K., Muench, R. D., Gunn, J., Björk, G., Rudels, B., … Schauer, U. (2001). The Arctic Ocean boundary current along the Eurasian slope and the adjacent Lomonosov ridge: Water mass properties, transports and transformations from moored instruments. *Deep. Res. Part I Oceanogr. Res. Pap.*, *48*(8), 1757–1792. doi: 10.1016/S0967-0637(00)00091-1

Zhang, J., Steele, M., Runciman, K., Dewey, S., Morison, J., Lee, C., … Toole, J. (2016, nov). The Beaufort Gyre intensification and stabilization: A model-observation synthesis. *J. Geophys. Res. Ocean.*, *121*(11), 7933–7952. doi: 10.1002/2016JC012196

Zhong, W., & Zhao, J. (2014). Deepening of the Atlantic Water core in the Canada basin in 2003-11. *J. Phys. Oceanogr.*, *44*(9), 2353–2369. doi: 10.1175/JPO-D-13-084.1